Ultrafast and Precise Interrogation of Fiber Bragg Grating Sensor Based on Wavelength-to-Time Mapping Incorporating Higher Order Dispersion

Haiyun Xia, *Student Member, OSA*, Chao Wang, *Student Member, IEEE, OSA*, Sébastien Blais, *Student Member, IEEE*, and Jianping Yao, *Senior Member, IEEE, Fellow, OSA*

***Abstract*—An interrogation scheme based on wavelength-to-time mapping to achieve ultrafast, high-precision, and large dynamic range interrogation of fiber Bragg grating (FBG) sensors is proposed and experimentally demonstrated. The wavelength-to-time mapping, also called temporal self-imaging effect, is realized in the optical domain, using a dispersive element that has a large group velocity dispersion. For a practical dispersive element, higher order dispersions exist, which makes the wavelength-to-time mapping nonlinear. Thus, an interrogation system based on wavelength-to-time mapping without considering the high-order dispersion would reduce the interrogation accuracy. In this paper, for the first time to the best of our knowledge, a mathematical model that incorporates higher order dispersion to achieve an accurate wavelength-to-time mapping is developed, which is then verified by a numerical simulation. An FBG-based strain sensor interrogated based on the developed wavelength-to-time mapping scheme is experimentally investigated. The system has a sampling speed of 48.6 MHz, a dynamic range as large as 20 nm, and a sensing accuracy as high as 0.87 $\mu\varepsilon$ for a single-shot measurement.**

***Index Terms*—Femtosecond fiber laser, fiber Bragg grating (FBG), higher order dispersion, real-time dispersive Fourier transformation.**

I. Introduction

OPTICAL sensors using a fiber Bragg grating (FBG) or an FBG array have been intensively investigated for the detection of physical, chemical, biomedical, or electrical parameters, which are usually transferred into the wavelength shift of the optical signal from an FBG or an FBG array. The advantages such as immunity to electromagnetic interference, high resistance to chemical corrosion, multiplexing capability, high durability, light weight, and capability to be embedded in composites make FBG sensors have a wide range of scientific and industrial applications [1]–[4].

According to the principle of wavelength determination, the interrogation techniques can be generally classified into three main categories. In the first category, a static frequency discriminator is used to convert the wavelength shift of an FBG signal into an intensity change or intensity spatial displacement. It could be the transmission variation of the FBG signal on an edge filter such as a Fabry–Perot interferometer [5] or a wavelength-division-multiplexed (WDM) fiber coupler [6]. It could also be the change of the spatial intensity distribution on a linear-array charge-coupled device (CCD) when the FBG signal is discriminated by a dispersive element such as a holographic grating [7]. Usually, there is a tradeoff between the measurement resolution and the dynamic range when using an edge filter. The use of a CCD device limits the working wavelength at the 900-nm range, making it impossible to use the low-cost optical components developed for optical communications at the 1550 nm window. In the second category, a tunable filter with a relative narrow passband is used to scan the FBG spectrum. The spectrum measured is a convolution between the transfer function of the filter and the FBG spectrum. The scanning filter can be a tunable Fabry–Perot interferometer [8], an acousto-optic filter [9], or an FBG-based optical filter [10]. Interrogation systems based on the scanning technique are sensitive to the intensity fluctuations in the received signal, which are introduced by the laser source and the environmental disturbance during the scanning process. Thus, it is not suitable for applications where a fast and large dynamic range interrogation is needed. The techniques in the third category are implemented based on optical interferometry. The FBG signal is interrogated by scanning an unbalanced two-arm interferometer, such as a Michelson interferometer [11], which yields a beat signal that usually has an audio frequency associated with the wavelength of the corresponding FBG. If the received signal is produced by a FBG array, then the detector output contains a number of discrete audio frequencies with each corresponding to the particular FBG. If the interferometer is optimized to have a particular optical path difference (OPD) between the two arms and works at a static state, the frequency shifts of the FBG signal can be converted into the phase changes of the received signal [12].

In this paper, we propose and demonstrate a technique to interrogate an FBG sensor based on wavelength-to-time mapping incorporating higher order dispersion, which provides an ultrafast interrogation speed, large dynamic range, and high precision. The key significance of the technique is to use the wave-

Manuscript received August 03, 2009; revised November 22, 2009. First published December 04, 2009; current version published January 15, 2010. This work was supported by the Natural Sciences and Engineering Research Council of Canada through its Strategic Grants Program. The work of H. Xia was supported by a scholarship from the China Scholarship Council.

H. Xia is with the Microwave Photonics Research Laboratory, School of Information Technology and Engineering, University of Ottawa, Ottawa, ON K1N 6N5, Canada, and also with the Institute of Optoelectronics Engineering, Beijing University of Aeronautics and Astronautics, Beijing 100083, China.

C. Wang, S. Blais, and J. Yao are with the Microwave Photonics Research Laboratory, School of Information Technology and Engineering, University of Ottawa, Ottawa, ON K1N 6N5, Canada (e-mail: jpyao@site.uottawa.ca).

Color versions of one or more of the figures in this paper are available online at http://ieeexplore.ieee.org.

Digital Object Identifier 10.1109/JLT.2009.2037722

length-to-time mapping [13], [14] to convert the spectrum of an FBG or FBG array from the wavelength domain to the time domain. Since the temporal information can be processed with a higher resolution, the use of the proposed technique in an FBG sensor system would significantly increase the interrogation accuracy. In addition, in performing the wavelength-to-time mapping, higher order dispersion is considered, which would further increase the interrogation accuracy. Furthermore, since the wavelength-to-time mapping is implemented in real time and a good SNR is guaranteed by using a mode-locked femtosecond pulsed laser, a single-shot measurement without performing any averaging is feasible; therefore, the sensing system can operate at an ultrafast speed determined by the repetition rate of the pulsed laser source. Moreover, a large dynamic range is also ensured due to the broad spectral range of the ultrashort pulse source.

Wavelength-to-time mapping or real-time dispersive Fourier transformation implemented based on a coherent ultrashort pulsed light source has been widely used for optical signal processing. For example, it has been employed in optical coherence tomography or optical frequency-domain reflectometry [15]–[20] and real-time spectroscopy [21], [22].

The chromatic dispersion of a dispersion-compensating fiber (DCF) has been used in an interrogation system for an FBG sensor array [23], in which the DCF was considered as a linear wavelength-dependent time delayer. After a round-trip pass through the DCF, the signals reflected from the FBGs in the array arrive at the photodetector (PD) with different time delays, which are dependent on the center wavelengths of the reflected optical signals. However, the time-delay difference (TDD) between two pulses reflected from two neighboring FBGs is the sum of the round-trip light flying time between the two FBGs and the wavelength-dependent TDD introduced by the DCF. Thus, the environmental disturbance on the connecting fiber preceding a particular FBG would degrade the measurement accuracy. In addition, it was assumed that the frequency-to-time mapping is linear, and the phase of the ultrashort optical pulse was not considered, which would introduce systematic errors into the interrogation. All these factors lead to a strain resolution of about $\pm 20\ \mu\varepsilon$ [23]. In this paper, these problems are solved by using the transmission spectrum from the FBG array, and the frequency-to-time mapping is used incorporating higher order dispersion.

In addition to the incorporation of high-order dispersion in the wavelength-to-time mapping to improve the interrogation accuracy, in the proposed approach, the FBGs are used in transmission instead of reflection. A transmission FBG can be designed to have a lower reflection with a shorter physical length, which could increase the spatial resolution.

Frequency-to-time mapping can also be implemented based on an incoherent pulse source [24]. The operation could be explained using the temporal van Cittert-Zernike theorem [25]. However, the sensitivity of such implementation is much less than that of the coherent implementation [25].

The paper is organized as follows. In Section II, the real-time Fourier transformation using a dispersive element incorporating higher order dispersion is discussed. In Section III, a simulation is performed to show the impact of higher order dispersion on the interrogation accuracy of FBG sensors. In Section IV, two experiments are carried out with the first experiment for the calibration of the sensing system and the second experiment for the measurement of the strain. The spectral resolution is defined and discussed. The measurement accuracy of the system is also evaluated. In Section V, a conclusion is drawn.

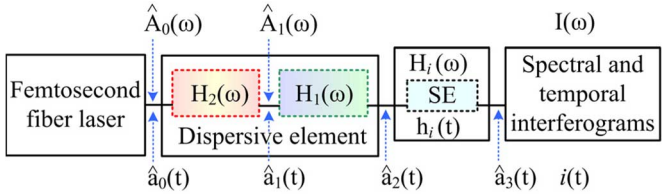

Fig. 1. Process for the analysis of wavelength-to-time mapping, using a dispersive element with higher order dispersion. SE: sensing element.

II. Principle

It is known that real-time frequency-to-time mapping can be achieved by using a dispersive element with a linear dispersion. For practical applications however, a dispersive element has higher order dispersion. In an interrogation system, if a linear frequency-to-time mapping function is used without considering the higher order dispersion, the interrogation accuracy would be reduced. In this section, we will derive a new frequency-to-time mapping function that incorporates higher order dispersion.

To build an accurate wavelength-to-time mapping function incorporating higher order dispersion, we start with an analysis of the propagation of an ultrashort pulse in a dispersive element with a large group velocity dispersion (GVD) and dispersion up to the third-order dispersion (TOD). The process to be followed for our discussion is shown in Fig. 1.

An ultrashort pulse source has a complex spectrum of

$$\hat{A}_0(\omega) = A_0(\omega)\exp[j\varphi_0(\omega)] = \tilde{F}[\hat{a}_0(t)] \tag{1}$$

where $\tilde{F}$ denotes the Fourier transform operation, $\hat{a}_0(t)$ is the complex envelope of the temporal pulse, and $A_0(\omega)$ and $\varphi_0(\omega)$ are the amplitude and phase of the pulse, respectively. The intensity spectrum is $I_0(\omega) = |A_0(\omega)|^2$.

If we consider the dispersion up to the TOD, the transfer function of the dispersive element, such as a length of dispersive fiber, can be expressed by expanding the mode-propagation constant β in Taylor series

$$\hat{H}(\omega) = \underbrace{H_0(\omega)\exp\left(-j\sum_{n=0}^{2}\frac{\beta_n L}{n!}\omega^n\right)}_{H_1(\omega)} \times \underbrace{\exp\left(-j\frac{\beta_3 L}{6}\omega^3\right)}_{H_2(\omega)} \tag{2}$$

where β_n is the nth order mode-propagation constant, $H_0(\omega)$ is a constant, which is unity if the loss of the dispersive fiber is ignored, ω is the angular frequency relative to the center frequency of the ultrashort pulse, and L is the length of the dispersive fiber. If the pulse power is small, no nonlinear phenomena

would occur in the dispersive fiber; thus, the entire system can be modeled as a linear time-invariant (LTI) system. The transfer function of the dispersive fiber can be considered as a cascade of two sub LTI systems, i.e., $H_1(\omega)$, the transfer function associated with the dispersion up to the GVD, and $H_2(\omega)$, the transfer function associated with the TOD, as shown in Fig. 1.

For simplicity, in the theoretical analysis, the sensing element (SE) is assumed to be a two-tap interferometer. We will show in the next session, the SE can be an FBG or an FBG array. The transfer function of a two-tap interferometer is given by

$$H_i(\omega) = [1 + \cos(\omega\tau)]/2 \tag{3}$$

where τ is the TDD between the two taps. The impulse response of the two-tap interferometer is

$$h_i(t) = [\delta(t) + \delta(t+\tau)]/2 \tag{4}$$

where $\delta(t)$ is the Dirac delta function.

As the first step, we need to know the complex envelope of the pulse after passing through the dispersive fiber. Since the system under analysis is an LTI system, the order of the transfer functions associated with the GVD, the TOD and the two-tap interferometer could be changed without affecting the total response of the system. The transfer function associated with the TOD of the dispersive fiber is

$$H_2(\omega) = \exp\left(-j\frac{\beta_3 L}{6}\omega^3\right). \tag{5}$$

First of all, we consider only the effect of the TOD in the dispersive fiber, the complex spectrum is

$$\hat{A}_1(\omega) = \hat{A}_0(\omega)H_2(\omega) = A_0(\omega)\exp[j\psi(\omega)] \tag{6}$$

where $\psi(\omega) = \varphi_0(\omega) - \beta_3 L\omega^3/6$.

The impulse function associated with the GVD in the dispersive fiber is the inverse Fourier transformation of $H_1(\omega)$, which can be expressed as

$$h_1(t_R) = h_0 \exp\left(jt_R^2/2\beta_2 L\right) \tag{7}$$

where $t_R = t - \beta_1 L$ is the time measured relative to the average time delay, and $h_0 = H_0(j2\pi\beta_2 L)^{-1/2}\exp(-j\beta_0 L)$ is the complex amplitude. Therefore, as shown in Fig. 1, the complex envelope $\hat{a}_2(t)$ of the output pulse at the end of the dispersive fiber can be expressed as a convolution between $\hat{a}_1(t)$ and $h_1(t_R)$

$$\begin{aligned}\hat{a}_2(t) &= h_1(t_R) * \hat{a}_1(t)\\ &= \int_{-\infty}^{\infty} h_0 \exp\left[\frac{j(t_R - t')^2}{2\beta_2 L}\right]\hat{a}_1(t')dt'\\ &= h_0 \exp\left(\frac{jt_R^2}{2\beta_2 L}\right)\int_{-\infty}^{\infty}\exp\left(\frac{jt'^2}{2\beta_2 L}\right)\\ &\quad\times \hat{a}_1(t')\exp\left(-\frac{jt_R t'}{\beta_2 L}\right)dt'\end{aligned} \tag{8}$$

where $*$ denotes the convolution operation. If the ultrashort pulse source and the dispersive fiber adopted have parameters to meet the temporal Fraunhofer condition $|t_0^2/2\beta_2 L| \ll 1$, where t_0 is the pulse duration, (8) can be approximated by

$$\begin{aligned}\hat{a}_2(t) &= h_0 \exp\left(\frac{jt_R^2}{2\beta_2 L}\right)\int_{-\infty}^{\infty}\hat{a}_1(t')\exp\left(-\frac{jt_R t'}{\beta_2 L}\right)dt'\\ &= h_0 \exp\left(\frac{jt_R^2}{2\beta_2 L}\right)[\hat{A}_1(\omega')]\end{aligned} \tag{9}$$

From (6) and (9), one can see, under the temporal Fraunhofer condition, the dispersive fiber acts as a frequency-to-time mapper, i.e., the output complex envelope $\hat{a}_2(t)$ is proportional to the complex spectrum $\hat{A}_1(\omega)$, with an angular frequency given by $\omega' = t_R/\beta_2 L$.

We note that the TOD introduces a frequency chirp to the original ultrashort pulse. To study this effect on the wavelength-to-time mapping, we analyze the relationship between the temporal interferogram and the spectral interferogram.

The electrical field of the optical signal at the output of the interferometer is given by

$$\hat{a}_3(t) = \hat{a}_2(t) * h_i(t). \tag{10}$$

Then the temporal interferogram can be written as

$$\begin{aligned}i(t) &= \Re\hat{a}_3(t)\overline{\hat{a}_3(t)}\\ &= \frac{\Re|h_0|^2}{4}\left\{|\hat{A}_1(\omega')|^2 + |\hat{A}_1(\omega'+\Delta\omega')|^2\right.\\ &\quad + 2|\hat{A}_1(\omega')||\hat{A}_1(\omega'+\Delta\omega')|\\ &\quad\left.\times\cos\left[\omega'\tau + \frac{\partial\psi(\omega')}{\partial\omega'}\Delta\omega'\right]\right\}\end{aligned} \tag{11}$$

where $\Re$ is the responsivity of the PD, $\overline{\hat{a}_3(t)}$ is a complex conjugate of $\hat{a}_3(t)$, and $\Delta\omega' = \tau/\beta_2 L$ is the corresponding frequency shear due to the TDD introduced by the interferometer. If $\Delta\omega'$ is small enough, (11) can be approximated by

$$\begin{aligned}i(t) &= \frac{1}{2}\Re|h_0|^2 I_0(\omega')\\ &\quad\times\left\{1 + \cos\left[\omega'\tau + \frac{\partial\psi(\omega')}{\partial\omega'}\Delta\omega'\right]\right\}.\end{aligned} \tag{12}$$

We study the phase of the cosine term in (12), which can be expressed as

$$\Theta(\omega') = \omega'\tau + \Delta\varphi_0(\omega') - \frac{\beta_3 L\omega'^2}{2}\Delta\omega'. \tag{13}$$

The femtosecond pulses generated by a passively mode-locked laser are nearly transform limited. Therefore, we have $\Delta\varphi_0(\omega') \approx 0$, then (13) can be approximated by

$$\begin{aligned}\Theta(\omega') &= \omega'\tau - \frac{\beta_3 L\omega'^2}{2}\Delta\omega'\\ &= \left(\frac{t_R}{\beta_2 L}\right)\tau - \frac{\beta_3 L}{2}\left(\frac{t_R}{\beta_2 L}\right)^2\left(\frac{\tau}{\beta_2 L}\right)\\ &= \omega''\tau\end{aligned} \tag{14}$$

where $\omega'' = t_R/\beta_2 L - \beta_3 L t_R^2/2(\beta_2 L)^3$.

Using the same process described earlier, the effect of higher order dispersion can be considered in the dispersive Fourier

transformation, which yields a general form of the angular frequency as a polynomial function of t_R.

$$\omega'' = \frac{t_R}{\beta_2 L} - \sum_{n=3}^{\infty} \frac{\beta_n L t_R^{n-1}}{(n-1)!(\beta_2 L)^n}. \tag{15}$$

Substituting (15) into (14), the function of the temporal interferogram becomes

$$i(t) = \Re|h_0|^2 I_0(\omega')[1+\cos(\omega''\tau)]/2. \tag{16}$$

In the frequency domain, the spectral interferogram can be expressed as a product of the pulse spectrum and the transfer function of the interferometer

$$I(\omega) = \Re I_0(\omega)[1+\cos(\omega\tau)]/2. \tag{17}$$

Comparing (16) and (17), one can find that the temporal interferogram is in analogy to the spectral interferogram, with a frequency–time relationship given by (15). Considering that the FBG signals are usually analyzed in the wavelength domain, (15) can be expressed as

$$2\pi c\left(\frac{1}{\lambda} - \frac{1}{\lambda_0}\right) = \frac{t_R}{\beta_2 L} - \sum_{n=3}^{\infty} \frac{\beta_n L t_R^{n-1}}{(n-1)!(\beta_2 L)^n} \tag{18}$$

where c is the light velocity in vacuum, and λ_0 is the center wavelength of the femtosecond pulse. From (16), (17), and (18), we know that the spectral information can be recorded not only in the wavelength domain but also in the time domain.

III. Numerical Simulation

To see the effect of higher order dispersion on the interrogation accuracy of an FBG sensor, a simulation is performed, in which a software package (Optiwave OptiSystem 6.0) is used. The femtosecond laser source has a bandwidth of 3.3 THz with a center frequency of 193 THz. In the simulation, the interferometer in Fig. 1 is substituted by an FBG array, which consists of five uniform FBGs with an identical reflectivity of 0.4 and a bandwidth of 1.2 nm. These FBGs locate symmetrically about the center wavelength of the femtosecond pulse with a wavelength interval of 4 nm, as shown in Fig. 2(a). For an easy comparison with the temporal waveform, the spectrum is flipped vertically. The dispersive element is a 12-km standard single-mode fiber with a dispersion parameter of $D = 16.75$ ps/nm/km. The femtosecond pulse transmitting through the FBG array is fed to a 50-GHz PD, and the output is recorded using an oscilloscope (OSC).

Two cases are considered. In the first case, it is assumed the higher order dispersion is zero in the single-mode fiber. In the second case, the dispersion slope of the single-mode fiber is assumed to be 0.6 ps/nm^2/km. The temporal waveforms corresponding to both cases are shown in Fig. 2(b). As expected, both temporal waveforms are in analogy to the spectrum. But, when the TOD is considered, the envelope of the temporal waveform becomes distorted. One can see that, in this case, the slots associated with FBGs locating on the leading edge of the waveform slide toward the center of the femtosecond pulse. On the contrary, the slots associated with FBGs locating on the trailing edge deviate from the center. Therefore, to perform an accurate wavelength-to-time mapping, the higher order dispersion should not be ignored.

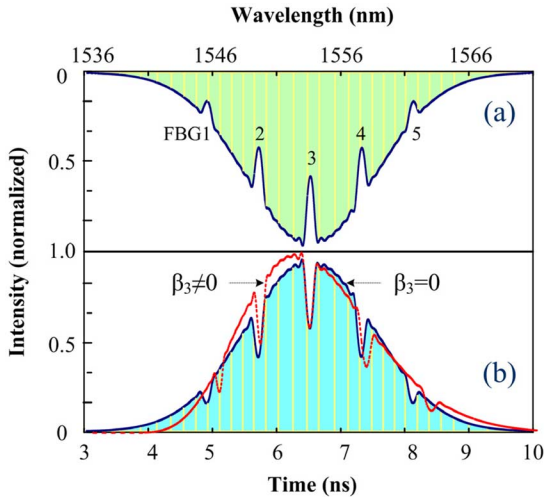

Fig. 2. Simulation results: (a) the spectrum of the femtosecond pulse after transmitting through the FBG array, (b) the waveforms without (solid line), and with (dotted line) TOD.

IV. Experiment

The schematic diagram of the FBG sensor interrogation system is shown in Fig. 3. It consists of four sub-systems, i.e., the optical source, the sensor module, the calibration module, and the optical receiver. The optical source is a passively mode-locked femtosecond fiber laser (IMRA Femtolite 780 Model B-4-FC-PD), which emits a train of pulses with a pulsewidth of 394 fs (full-width at half-maximum) and a center frequency of 192.31 THz at a repetition rate of 48.6 MHz. A variable optical attenuator (VOA) is used to control the optical power to avoid any nonlinear phenomena in the system. In the sensor module, to demonstrate that WDM technique is easy to be incorporated in our system, five FBGs with different center wavelengths are written in cascade in an optical fiber, using different uniform phase masks, all with a Gaussian apodization. FBG_0 is set free of tensile strain and placed close to other FBGs to compensate for the wavelength shift corresponding to the environmental temperature change. Other four FBGs are stretched by using a piezoelectric transducer (PZT) (PI Model P-752.1CD), which is driven by a PZT controller (PI Model E-665.CR). The piezoelectric system works in a servo-control mode based on the integrated feedback capacitive sensor, which provides an accuracy of 0.2 nm. To perform an accurate tensile strain measurement, both ends of the FBG array are glued to metal sticks with epoxy and then cased with thermal shrink tube, as shown in Fig. 4(c).

According to (18), since both the PD and the OSC have a limited temporal resolution in the optical receiver; the accumulated GVD should be as large as possible to achieve a high resolution in the wavelength domain. In the experiment, two coils of dispersion compensating fiber DCF_1 and DCF_2 are used in cascade to stretch the femtosecond pulses sufficiently in the time domain, which provide a GVD about -952.4 ps/nm. To ensure a good SNR, two erbium-doped fiber amplifiers (EDFA) are used

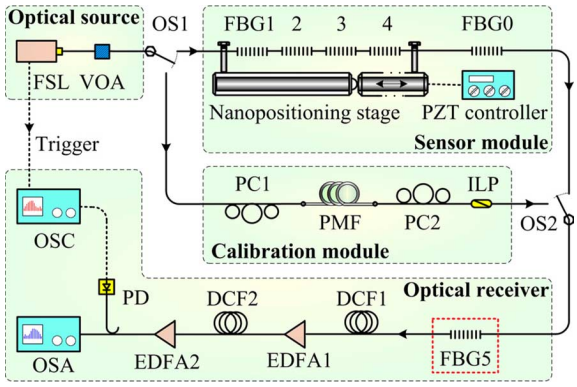

Fig. 3. (Color online) schematic diagram of the proposed system. FSL, femtosecond pulse laser; VOA, variable optical attenuator; OS, optical switch; PZT, piezoelectric transducer; PC, polarization controller; PMF, polarization maintaining fiber; ILP, in-line polarizer; DCF, dispersion compensation fiber; EDFA, erbium doped fiber amplifier; PD, photodetector; OSC, oscilloscope; OSA, optical spectrum analyzer.

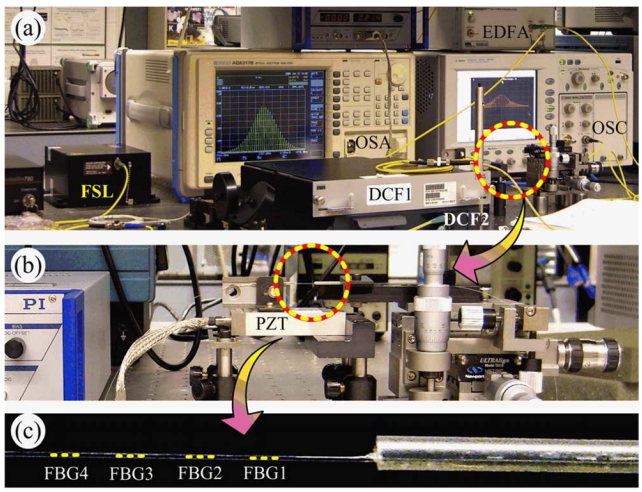

Fig. 4. (Color online) picture of the prototype. (a) Entire system, (b) sensor module, and (c) FBGs under tensile stretch.

in cascade in the system. The temporal interferogram and the spectral interferogram are recorded using an OSC and an optical spectrum analyzer (OSA), respectively. The sixth FBG, FBG_5, that experiences null strain and null temperature change is used as a reference, upon which all the sensing results can be calibrated. Furthermore, FBG_5 provides a time-invariant reference point for the time-to-wavelength conversion. The corresponding coordinates for FBG_5 are [0 ns, 1557.985 nm]. If a high SNR is achieved by averaging waveforms over a period of time, all the waveforms recorded on the OSC at different time within the period should be aligned to the peak of FBG_5 first.

To establish the wavelength-to-time relationship, a calibration module is incorporated into the entire system by using two optical switches OS_1 and OS_2. The key element of the calibration module is a polarization-maintaining fiber (PMF). By adjusting the polarization controller (PC), PC_1, the incoming light wave is decomposed equally into two orthogonally polarized components along the fast and slow axes of the PMF and then propagate at different velocities; therefore, a TDD is introduced between the two orthogonally polarized components. The

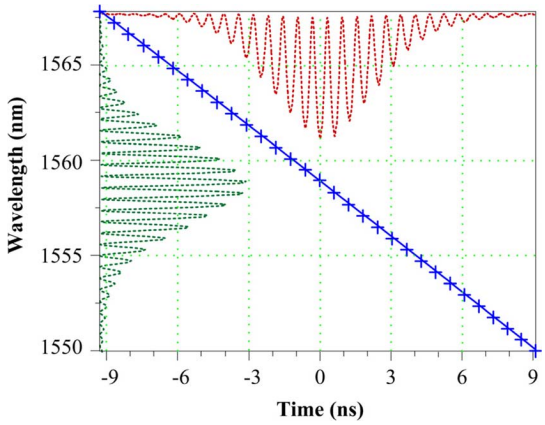

Fig. 5. Wavelength-to-time conversion function.

second PC, PC_2, preceding the in-line polarizer (ILP) is used to optimize the fringe visibility in the interferogram.

In the first experiment, the calibration module is connected to the system. Interferograms in the wavelength domain and in the time domain are recorded by using the OSA and the OSC, which are shown in Fig. 5 along the vertical and the horizontal axes, respectively. The center frequencies of the peaks in both interferograms are found, which are used to fit to a polynomial function given by

$$\lambda = 1557.985 - 1.046t - 7.728 \times 10^{-4}t^2 - 1.738 \times 10^{-5}t^3 \quad (19)$$

where the unit of wavelength is in nanometer, and the unit of time is in nanosecond. In the following experiment, (19) is used to transform the temporal waveform into its corresponding spectrum. This calibration is valid only if the difference of integral dispersion between the sensor module and the calibration module is negligible when comparing to the dispersion provided by the dispersive element. Fortunately, if we write enough FBGs over the spectrum of the femtosecond pulse, a self-calibration can be performed by building a relationship between the FBG slots in the temporal waveform and its corresponding spectrum, as shown in the simulation in Section III.

In the second experiment, the sensor module is connected to the system. To perform an accurate measurement, we add a prestrain to the FBG array by adjusting a precise optic fiber stage at the right end of the FBG array, as shown in Fig. 4(b). The FBG array is measured to have a length of 13.96 cm, and the PZT has a resolution of 0.2 nm, thus the strain added to the FBG array has an accuracy of 1.43 nε. The PZT is set to have 17 steps with an increment of each step of 2 μm. The spectrums recorded on the OSA and the temporal waveforms recorded on the OSC are aligned to the center of the reference FBG_5, as shown in Fig. 6. Since the sign of the GVD of the dispersive fiber is a minus, the temporal waveforms are flipped horizontally relative to the spectra. In the following discussion, instead of using the spectra recorded on the OSA, the strain information is retrieved from the temporal waveforms recorded on the OSC.

The temporal displacement of the peaks versus the strain added to the FBG array is shown in Fig. 7(a) as a contour map. We find that due to the higher order dispersion associated with

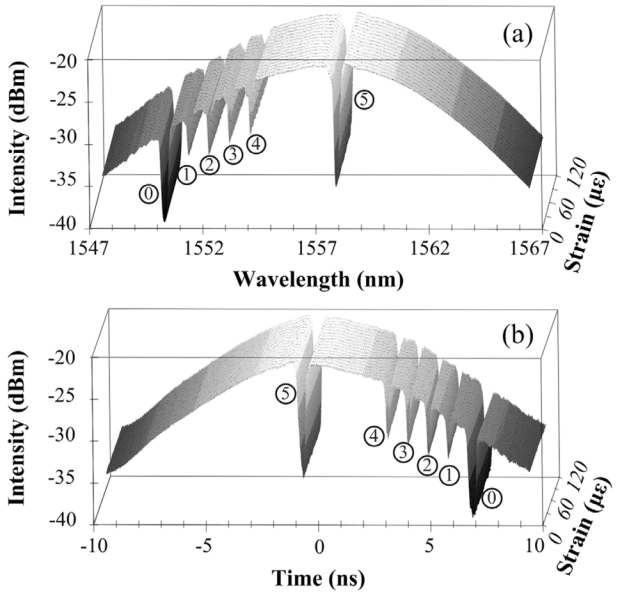

Fig. 6. Experimental results: (a) transmission spectrum of the femtosecond laser pulse after passing through the FBG array under different tensile strain and (b) temporal waveforms recorded on the OSC.

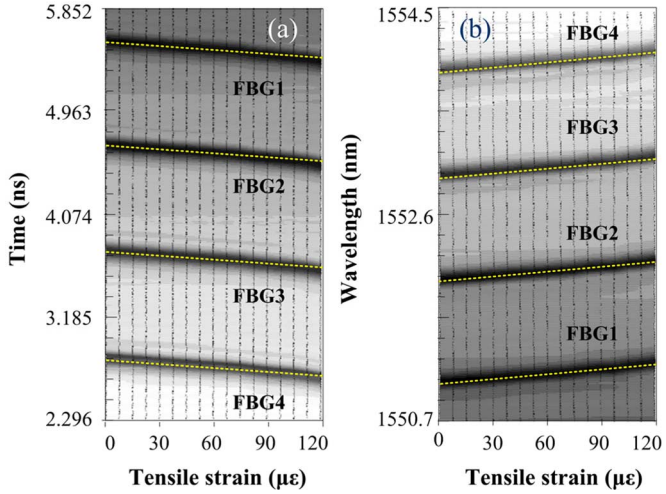

Fig. 7. (a) Contour map of the temporal waveforms and (b) contour map the spectra in the wavelength domain obtained from (a) using (18).

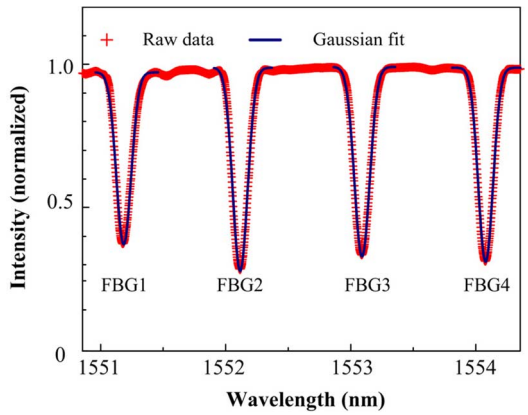

Fig. 8. Measurement of the center wavelength of each FBG. Each selected part of the curve is fitted to a Gaussian function.

the dispersive fiber, the FBG shifting contrails corresponding to the change of tensile strain deviate from the straight lines slightly in Fig. 7(a). As the first step of the data processing, Fig. 7(a) is transformed from the time domain into the wavelength domain, using (19), as shown in Fig. 7(b). Since the femtosecond laser pulse has a Gaussian profile in the wavelength domain, the intensity of the contour map in Fig. 7(b) is easy to be normalized. Then, the selected part of the normalized spectrum associated with each single FBG is fitted to a Gaussian function to decide the center wavelength, as shown in Fig. 8. In this figure, the temperature disturbance is compensated by a direct subtraction of the wavelength shift of FBG_0 relative to FBG_5. The wavelength-strain sensitivity corresponding to $\mathrm{FBG}_1, \mathrm{FBG}_2, \mathrm{FBG}_3$, and FBG_4 are measured to be 1.257, 1.259, 1.258, and 1.261 pm/$\mu\varepsilon$, respectively. The nominal wavelengths and the reflectivities of the six FBGs from FBG_0 to FBG_5 are (1550.173 nm, 0.9072), (1551.129 nm, 0.6259), (1552.061 nm, 0.7169), (1553.035 nm, 0.6658), (1554.023 nm, 0.6865), and (1557.985 nm, 0.9776), respectively.

According to (19), as a DCF is used, for a femtosecond pulse with a temporal width of more than 20 ns (corresponding to a spectral width of 21 nm), the actual frequency-to-time mapping function could deviate from a linear wavelength-to-time function of about 0.3 nm, which would introduce a strain error as large as 238 $\mu\varepsilon$.

To evaluate the accuracy of the system, we preset the PZT to two different steps, thus a change of tensile strain is applied to the FBG array.

For sensor applications, what we are interested is the detectable minimum wavelength shift. Therefore, in this paper, the spectral resolution is defined as the detectable minimum wavelength shift of the FBG profile, which is different from the work in [21], [22], where the spectral resolution is defined as the distinguishable minimum separation between two gas absorption lines. The difference lies in the fact that a FBG can be designed to have a broader spectrum with more normal shape relative to a gas absorption line.

It is obvious that, from (18), given a limited temporal resolution of the receiver, the higher the dispersion $\beta_2 L$, the higher the sensitivity of the system. However, the duration of the stretched pulses should not exceed the repetition period of the femtosecond fiber laser (20.6 ns) to avoid the temporal overlap of two neighboring pulses. Considering that the femtosecond pulse has a spectrum extending to about 20 nm, a dispersion of -952.4 ps/nm is used. A PD (New Focus Model 1014, 45 GHz bandwidth) and a real-time OSC (Tektronix Model TDS7704B, 7 GHz bandwidth, 20 Gs/s) are used to capture and digitize the waveform. The FBGs used for strain measurement are designed to have a Gaussian profile and a spectral width (full-width at half-maximum) of about 0.2 nm. Thus, for a particular FBG spectrum dispersed in the time domain, more than 14 sampling data within 700 ps around the peak value can be selected to reconstruct the waveform. The temporal broadening of the waveform due to the PD is considered to be negligible since its rise time is only about 8 ps. The highest temporal resolution of the OSC is about 1 ps, which equals to a wavelength resolution of about 1.046 pm and a strain resolution of 0.83 $\mu\varepsilon$ according

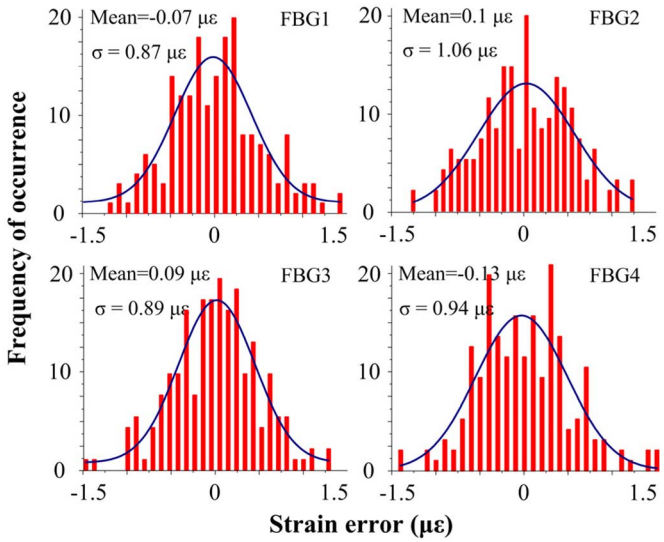

Fig. 9. Histograms of the difference between the preset strain and the strain value measured using the proposed system. The measurement number is 194.

to (19). In this experiment, the sampling data are interpolated by the OSC to 1 ps/point automatically before being fed to the computer. The real-time OSC can record 4-μs signals within one frame, which contains 194 recorded temporal spectrums. Then, the recorded waveform is transformed into its spectrum using (19) and normalized to the Gaussian profile of the femtosecond pulse. To decide the wavelength center, 700 sampling points around the peak value of each FBG on the normalized transmission curve are selected and fitted to a Gaussian function.

$$G(\lambda) = B_c - (A/W\sqrt{\pi/2})\exp\{-2[(\lambda-\lambda_c)/W]^2\} \quad (20)$$

where B_c is an offset, A is the area under the curve, λ_c is the wavelength center, and W is the spectral width of the FBG. Numerical least-squares Gaussian fitting is performed based on the Levenberg–Marquardt algorithm. Then, the difference of strain detection can be calculated by comparing the preset strain and the measured value. The histograms presented in Fig. 9 summarize the calculated results associated with the four FBGs. The measurement errors are estimated using the normal distribution. The mean difference varies from 0.07 to 0.13 $\mu\varepsilon$, and the standard error varies from 0.87 to 1.06 $\mu\varepsilon$.

V. Conclusion

We have proposed and experimentally demonstrated a new scheme using real-time wavelength-to-time mapping in a dispersive element with a high GVD for ultrafast and high-precise interrogation of an FBG sensor. A multipoint single-shot tensile strain measurement was demonstrated by recording the transmission spectrum of a transform-limited femtosecond pulse through an FBG array in the time domain. Its inherent advantages, including ultrafast speed, high resolution, and large dynamic range, make it a promising technique for applications where ultrafast speed and high-accuracy sensing is needed in some harsh environment, e.g., the simultaneous detection of the temperature and vibration of a running aircraft turbine.

Compared with conventional FBG interrogation techniques based on a static frequency discriminator or a tunable filter where only one end of the FBG array needs to be accessed, the proposed technique may have limitations in terms of implementation flexibility and structure simplicity due to the fact the FBG or FBG array should be accessed from two sides. However, the proposed technique is superior in terms of multiplexing capacity, by virtue of the broad spectral width of the femtosecond pulse, more FBGs with different center wavelengths can be incorporated in the system, with an increased multiplexing capacity. In fact, the spectral width of a femtosecond pulse can be further extended using a highly nonlinear fiber, thus more FBG sensors can be simultaneously interrogated.

For a given bandwidth of the receiver, the GVD should be as large as possible to guarantee the measurement sensitivity, since the larger the bandwidth of the FBG sliced femtosecond spectrum, the wider it extends in the time domain. However, the overlap between two neighboring temporally dispersed pulses should be avoided, which would impose of an upper limit of the numbers of FBGs that can be incorporated in the system. In addition, if a large number of FBGs are used in the system in which the femtosecond pulse source is assumed to have an extremely broad spectrum, to avoid an overlap between two consequent pulses in the receiver, a maximum repetition rate of the femtosecond pulse should be given, which determines the highest speed of the interrogation.

Due to the high loss associated with the use of a long dispersive fiber to achieve real-time wavelength-to-time mapping, two EDFAs were incorporated in the system to compensate for the losses resulted from the long DCF, which makes the system bulky. The size can be significantly reduced if a linearly chirped FBG is used to replace the long DCF. Then, a more compact optical interrogation system with better stability is possible. We should note, however, the dispersion ripples in the linearly chirped FBG would have negative impact on the measurement accuracy. In such a case, the theoretical analysis performed in this paper becomes significant, since the dispersion ripples can be modeled as high-order dispersion, which is considered in the wavelength-to-time mapping process.

References

[1] A. D. Kersey, M. A. Davis, H. J. Patrick, M. LeBlanc, K. P. Koo, C. G. Askins, M. A. Putnam, and E. J. Friebele, "Fiber grating sensors," *J. Lightw. Technol.*, vol. 15, no. 8, pp. 1442–1463, Aug. 1997.
[2] Y. J. Rao, "In-fibre Bragg grating sensor," *Meas. Sci. Technol.*, vol. 8, no. 4, pp. 355–375, Apr. 1997.
[3] A. Othonos, "Fiber Bragg gratings," *Rev. Sci. Instrum.*, vol. 68, no. 12, pp. 4309–4341, Dec. 1997.
[4] S. Yin, P. B. Ruffin, and F. T. S. Yu, *Fiber Optic Sensors*, 2nd ed. Boca Raton, FL: CRC Press, 2008, ch. 7.
[5] H. Xia, C. Zhang, H. Mu, and D. Sun, "Edge technique for direct detection of strain and temperature based on optical time domain reflectometry," *Appl. Opt.*, vol. 48, pp. 189–197, Jan. 2009.
[6] M. A. Davis and A. D. Kersey, "All fiber Bragg grating strain sensor demodulation technique using a wavelength division coupler," *Electron Lett.*, vol. 30, no. 1, pp. 75–76, Jan. 1994.
[7] W. Ecke, I. Latka, R. Willsch, A. Reutlinger, and R. Graue, "Fibre optic sensor network for spacecraft health monitoring," *Meas. Sci. Technol.*, vol. 12, no. 7, pp. 974–980, Jul. 2001.
[8] A. D. Kersey, T. A. Berkoff, and W. W. Morey, "Multiplexed fiber Bragg grating strain sensor system with a fiber Fabry-Perot wavelength filter," *Opt. Lett.*, vol. 18, no. 16, pp. 1370–1372, Aug. 1993.

[9] M. G. Xu, H. Geiger, J. L. Archambault, L. Reekie, and J. P. Dakin, "Novel interrogation system for fiber Bragg grating sensors using an acousto-optic tunable filter," *Electron. Lett.*, vol. 29, no. 17, pp. 1510–1511, Aug. 1993.

[10] D. A. Jackson, A. B. Lobo Ribeiro, L. Reekie, and J. L. Archambault, "Simple multiplexing scheme for a fiber optic grating sensor network," *Opt. Lett.*, vol. 18, no. 14, pp. 1193–1195, Jul. 1993.

[11] M. A. Davis and A. D. Kersey, "Application of a fiber Fourier transform spectrometer to the detection of wavelength-encoded signals from Bragg grating sensors," *J. Lightw. Technol.*, vol. 13, no. 7, pp. 1289–1295, Jul. 1995.

[12] A. D. Kersey, T. A. Berkoff, and W. W. Morey, "Fiber optic Bragg grating sensor with drift-compensated high resolution interferometric wavelength shift detection," *Opt. Lett.*, vol. 18, no. 1, pp. 72–74, Jan. 1993.

[13] T. Jannson and J. Jannson, "Temporal self-imaging effect in single-mode fibers," *J. Opt. Soc. Amer.*, vol. 71, no. 11, pp. 1373–1376, Nov. 1981.

[14] T. Jannson, "Real-time Fourier transformation in dispersive optical fibers," *Opt. Lett.*, vol. 8, no. 4, pp. 232–234, Apr. 1983.

[15] M. Wojtkowski, V. J. Srinivasan, T. J. Ko, J. G. Fujimoto, A. Kowalczyk, and J. S. Duker, "Ultrahigh-resolution, high-speed, Fourier domain optical coherence tomography and methods for dispersion compensation," *Opt. Exp.*, vol. 12, no. 11, pp. 2404–2422, May 2004.

[16] S. Moon and D. Y. Kim, "Ultra-high-speed optical coherence tomography with a stretched pulse supercontinuum source," *Opt. Exp.*, vol. 14, no. 24, pp. 11575–11584, Nov. 2006.

[17] Y. Park, T.-J. Ahn, J.-C. Kieffer, and J. Azaña, "Optical frequency domain reflectometry based on real-time Fourier transformation," *Opt. Exp.*, vol. 15, no. 8, pp. 4598–4617, Apr. 2007.

[18] R. E. Saperstein, N. Alic, S. Zamek, K. Ikeda, B. Slutsky, and Y. Fainman, "Processing advantages of linear chirped fiber Bragg gratings in the time domain realization of optical frequency-domain reflectometry," *Opt. Exp.*, vol. 15, no. 23, pp. 15464–15479, Nov. 2007.

[19] K. Goda, D. R. Solli, and B. Jalali, "Real-time optical reflectometry enabled by amplified dispersive Fourier transformation," *Appl. Phys. Lett.*, vol. 93, no. 3, pp. 0311061–0311063, Jul. 2008.

[20] K. Goda, K. K. Tsia, and B. Jalali, "Serial time-encoded amplified imaging for real-time observation of fast dynamic phenomena," *Nature*, vol. 458, pp. 1145–1150, Apr. 2009.

[21] D. R. Solli, J. Chou, and B. Jalali, "Amplified wavelength-time transformation for real-time spectroscopy," *Nat. Photon.*, vol. 2, no. 1, pp. 48–51, Jan. 2008.

[22] J. Chou, D. R. Solli, and B. Jalali, "Real-time spectroscopy with subgigahertz resolution using amplified dispersive Fourier transformation," *Appl. Phys. Lett.*, vol. 92, no. 11, pp. 1111021–1111023, Mar. 2008.

[23] M. L. Dennis, J. U. Kang, T.-E. Tsai, I. N. Duling, III, and E. J. Friebele, "Grating sensor array demodulation by use of a passively mode-locked fiber laser," *Opt. Lett.*, vol. 22, no. 17, pp. 1362–1364, Sep. 1997.

[24] H. Y. Fu, H. L. Liu, X. Dong, H. Y. Tam, P. K. A. Wai, and C. Lu, "High-speed fibre Bragg grating sensor interrogation using dispersion-compensation fibre," *Electron. Lett.*, vol. 44, no. 10, pp. 618–619, May 2008.

[25] C. Dorrer, "Temporal van Cittert-Zernike theorem and its application to the measurement of chromatic dispersion," *J. Opt. Soc. Amer. B*, vol. 21, no. 8, pp. 1417–1423, Aug. 2004.

Haiyun Xia received the B.S. degree in physics and M.S. degree in optics from Soochow University, Suzhou, China, in 2003 and 2006, respectively. He is currently working toward the Ph.D. degree in optoelectronics as a joint training student in Beijing University of Aeronautics and Astronautics, Beijing, China and the Microwave Photonics Research Laboratory, School of Information Technology and Engineering, University of Ottawa, ON, Canada.

His current research interests include all-optical signal processing, ultrashort laser pulse characterization, laser remote sensing, and fiber-optic sensors.

Chao Wang (S'07) received the B.Eng. degree in opto-electrical engineering from Tianjin University, Tianjin, China, in 2002, and the MSc degree in optics from Nankai University, Tianjin, China, in 2005. He is currently working toward the Ph.D. degree in electrical engineering at the Microwave Photonics Research Laboratory, School of Information Technology and Engineering, University of Ottawa, Ottawa, ON, Canada.

His current research interests include microwave signal generation, radio-over-fiber systems, fiber Bragg grating, and their applications in microwave photonics systems.

Sebastien Blais (S'01) received the B.A.Sc. degree from the Université de Moncton, Moncton, NB, Canada, in 2003, and the M.S. degree in electrical engineering from the University of Ottawa, Ottawa, ON, Canada, in 2005. He is currently working toward the Ph.D. degree at the Microwave Photonics Research Laboratory, School of Information Technology and Engineering, University of Ottawa.

His research interests include fiber Bragg gratings, superstructured fiber Bragg gratings, photonic processing of microwave signals, optical waveguide devices, and phased array antennas.

Jianping Yao (M'99–SM'01) received the Ph.D. degree in electrical engineering from the Université de Toulon, Toulon, France, in 1997.

He joined the School of Information Technology and Engineering, University of Ottawa, Ontario, Canada, in 2001, where he is currently a Professor, Director of the Microwave Photonics Research Laboratory, and Director of the Ottawa-Carleton Institute for Electrical and Computer Engineering. From 1999 to 2001, he held a faculty position with the School of Electrical and Electronic Engineering, Nanyang Technological University, Singapore. He holds a Yongqian Endowed Visiting Chair Professorship with Zhejiang University, China. He spent three months as an Invited Professor in the Institut National Polytechnique de Grenoble, France, in 2005. His research has focused on microwave photonics, which includes all-optical microwave signal processing, photonic generation of microwave, millimeter-wave and THz, radio over fiber, UWB over fiber, fiber Bragg gratings for microwave photonics applications, and optically controlled phased array antenna. His research interests also include fiber lasers, fiber-optic sensors, and biophotonics. He has authored or co-authored over 140 papers in refereed journals and over 120 papers in conference proceeding.

Dr. Yao received the 2005 International Creative Research Award of the University of Ottawa. He was the recipient of the 2007 George S. Glinski Award for Excellence in Research of the University of Ottawa. He was named University Research Chair in Microwave Photonics in 2007. He was a recipient of a Natural Sciences and Engineering Research Council of Canada Discovery Accelerator Supplements award in 2008. He is an Associate Editor of the *International Journal of Microwave and Optical Technology*. He is on the Editorial Board of IEEE TRANSACTIONS ON MICROWAVE THEORY AND TECHNIQUES. He is a registered professional engineer of Ontario, Canada. He is a Fellow of the Optical Society of America and a Senior Member of IEEE Photonics Society and IEEE Microwave Theory and Techniques Society.